Controlling airborne cues to study small animal navigation

Marc Gershow[1], Matthew Berck[1], Dennis Mathew[2], Linjiao Luo[1], Elizabeth A Kane[1], John R Carlson[2] & Aravinthan D T Samuel[1]

Small animals such as nematodes and insects analyze airborne chemical cues to infer the direction of favorable and noxious locations. In these animals, the study of navigational behavior evoked by airborne cues has been limited by the difficulty of precisely controlling stimuli. We present a system that can be used to deliver gaseous stimuli in defined spatial and temporal patterns to freely moving small animals. We used this apparatus, in combination with machine-vision algorithms, to assess and quantify navigational decision making of *Drosophila melanogaster* larvae in response to ethyl acetate (a volatile attractant) and carbon dioxide (a gaseous repellant).

Olfaction is a sophisticated sensory modality. Odor plumes from sources in an animal's environment are carried and mixed by chaotic air currents before reaching an animal's olfactory organ. From a complex olfactory signal, and the resulting time-varying activity of a panel of olfactory neuronal types, an animal strives to locate and discriminate odor sources[1–3].

Olfactory computation may be studied using small invertebrates like *Caenorhabditis elegans* and *D. melanogaster*, which have small circuits and simple behaviors and are amenable to genetic manipulation[4,5]. Quantitative behavioral analysis, an important step in defining olfactory computations, is complicated by the difficulty of delivering precise airborne stimuli to freely moving animals. Classical behavioral assays for these animals quantify migration toward or away from droplets of odor[6–9]. In these assays, evaporation, convection and diffusion create spatially varying concentration gradients that change over time during each experiment. Droplet-based assays can be improved by calibrating the odor profile in closed plates using infrared spectroscopy[8,9]; however, gases such as carbon dioxide (CO_2) that are not liquid at room temperature cannot be used, spatial or temporal gradients cannot be precisely defined, the odor profile cannot be held stable in time, and a relatively small experimental arena must be used, leading to lower throughput. An alternative is to deliver waterborne stimuli using microfluidic devices engineered to the shape and movements of each animal. Such devices constrain behavior to their specific geometries[10–12] and do not easily accommodate many animals including insect larvae.

We present a device (**Fig. 1**) that allows us to deliver airborne cues in defined spatial and temporal gradients to freely behaving animals. An array of miniature solenoid valves injects odorant cues into a laminar airflow directed across an experimental arena. The amount of airborne cue injected at each point can be dynamically regulated during each experiment. This device generated long-lasting, stable and highly reproducible spatiotemporal gradients of any gas, including CO_2, a salient cue for *D. melanogaster* and *Anopheles* sp. mosquito[13,14], and features a large experimental arena that allows many small invertebrates to be studied simultaneously for extended periods of time.

Using our device, in combination with custom machine-vision software, the multianimal gait and track (MAGAT) analyzer (**Fig. 2** and **Supplemental Fig. 1**), we quantified navigational decision making of *D. melanogaster* larvae in response to airborne cues with higher precision and throughput than has been possible with earlier methods. We examined *D. melanogaster* larva chemotaxis to an airborne attractant (ethyl acetate) and repellant (CO_2) and discovered similarities between the larva's response to these gaseous cues and its navigation of thermal gradients.

RESULTS

Gradient generation

Our device creates airborne gradients in a square arena, 25 cm on a side, allowing extended observation of many animals per experiment and surpassing the throughput of single animal methods[8,15]. A slow laminar airflow (1.2 cm s^{-1}) is directed along the *y* axis of the arena. A row of miniature solenoid valves spaced 8 mm apart is used to generate gradients along the *x* axis. When each valve is open, a dose of gaseous cue is injected at a specific point along the *x* axis into the airflow. The opening of the valves and the odor-carrying airflow may be used to generate defined spatial and temporal gradients of any gaseous cue (Online Methods and **Supplementary Note 1**; detailed plans are available in **Supplementary Data**).

To characterize the gradients within the arena, we substituted its glass lid with an aluminum plate fitted with miniature gas detectors. We imposed a linear gradient by programming the fraction of time each valve was open to be in proportion to

[1]Department of Physics and Center for Brain Science, Harvard University, Cambridge, Massachusetts, USA. [2]Department of Molecular, Cellular and Developmental Biology, Yale University, New Haven, Connecticut, USA. Correspondence should be addressed to A.D.T.S. (samuel@physics.harvard.edu).

RECEIVED 24 AUGUST 2011; ACCEPTED 30 NOVEMBER 2011; PUBLISHED ONLINE 15 JANUARY 2012; DOI:10.1038/NMETH.1853

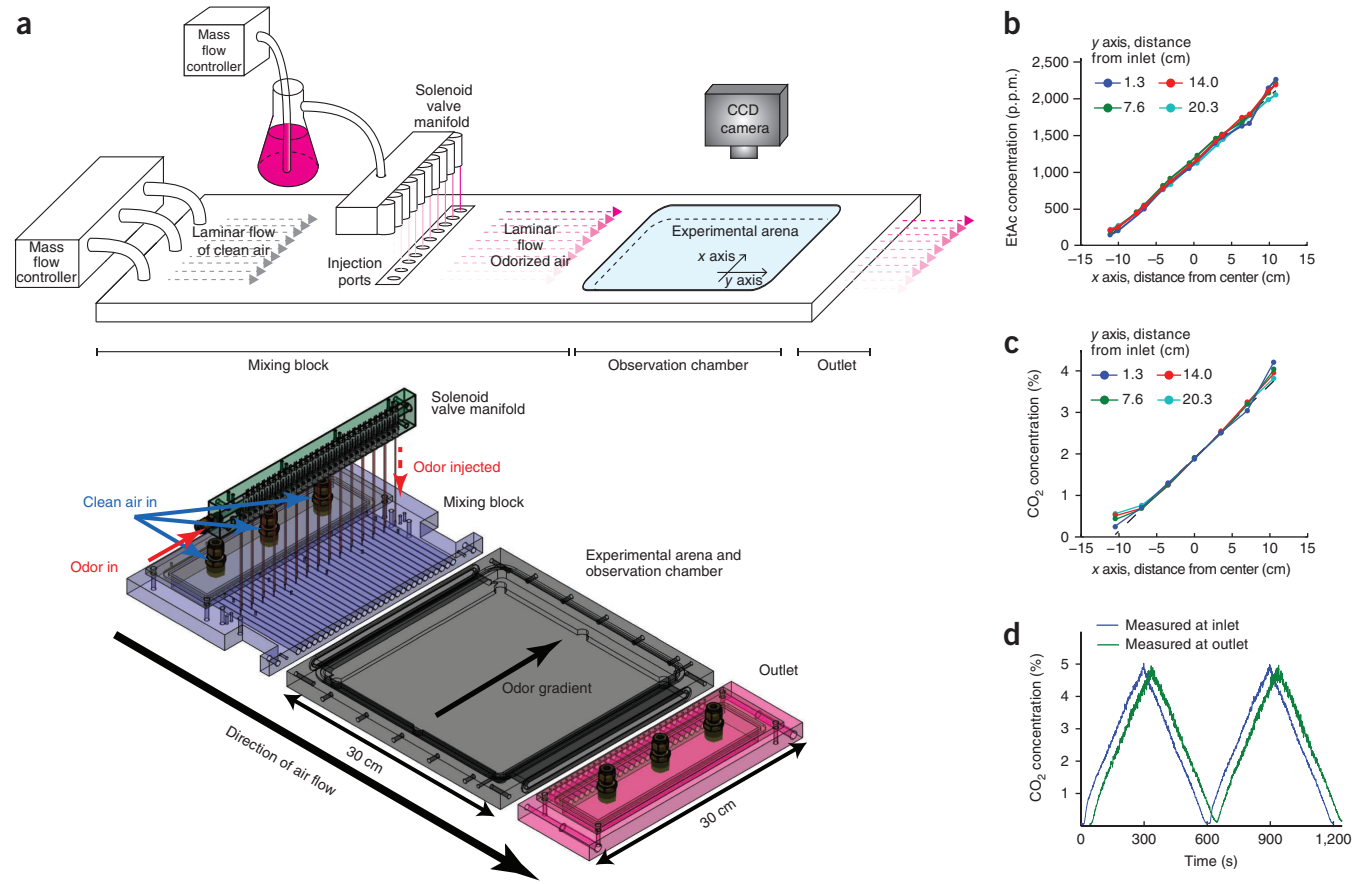

Figure 1 | Apparatus design and performance. (**a**) Schematic of the device (top). Clean airflow into the rear of the apparatus is regulated by a mass flow controller. For ethyl acetate experiments, a second mass flow controller controls airflow through a bubbler containing ethyl acetate. Odorized air is injected into points across the laminar airflow within a mixing block using a solenoid valve manifold. The laminar airflow odorized with a spatial gradient of ethyl acetate in the mixing block then passes into an observation chamber containing an experimental arena with transparent ceiling, allowing visualization of animal behavior inside the arena with a charge-coupled device (CCD) camera. Semitransparent isometric projection (bottom) of custom-machined components of the apparatus, including solenoid valve manifold, mixing block, experimental arena and observation chamber, and outlet. Direction of air flow (*y* axis) and gradient (*x* axis) are indicated. 'Odor gradient' arrow points to higher concentration in experiments described here. (**b**,**c**) Measurement of precision of linear spatial gradients of ethyl acetate (EtAc; **b**) or CO_2 (**c**) in the experimental arena. Gas concentration was measured at specific points in the experimental arena across the airflow (arena *x* axis) at indicated distances from the inlet (arena *y* axis). (**d**) CO_2 concentration at inlet and outlet during a 10-min temporal triangle ramp from 0% to 5% CO_2.

its position along the *x* axis. With either ethyl acetate or CO_2 (**Fig. 1b**,**c**), we found that the deviation from linearity was <3% of the mean concentration in the region in which the behavioral experiments were done.

To generate temporal gradients, we mixed odor into the airstream before it entered the device, controlling the odor flow rate into the airstream while monitoring odor concentration at the chamber inlet and outlet (**Supplementary Note 2** and **Supplementary Fig. 2** and **Fig. 1d**). The concentration is constant along the *x* axis, as the odor is mixed into the airstream before entry into the flow tubes that are used to define a spatial gradient. Along the *y* axis, the concentration varies as the time-varying odor profile is pushed across the chamber by the moving air flow. We measured a time lag between the detection of an odor change in the inlet and the outlet that corresponds to the flow rate of the gas in the chamber. Thus, the concentration at any point in the chamber is given by $C(y,t) = C_{\text{inlet}}(t - t_d - y / v_f)$, where v_f is the flow speed in the chamber and t_d is the time it takes gas to flow from the inlet to the flow chamber entrance.

Behavioral analysis

The trajectories of crawling *D. melanogaster* larvae are characterized by periods of forward movement (runs) that are interrupted by turns. We have previously used a high-resolution tracking microscope to follow individual *D. melanogaster* larvae on temperature gradients[15]. We have shown that a larva biases the frequency, direction and size of turns to move toward favorable temperatures. Here we sought to achieve the same resolution of behavioral analysis in a multianimal experiment. To do this, we developed the MAGAT analyzer software package to follow many larvae in parallel (**Supplementary Video 1**, **Supplementary Fig. 1** and **Supplementary Software 1;** software updates will be available at https://github.com/samuellab/MAGATAnalyzer) and determine the behavioral state of each larva (running, turning and sweeping the head) at all times (**Fig. 2a**,**b** and **Supplementary Note 3** and **Supplementary Videos 2**–**6**). The MAGAT analyzer quantifies the navigational performance of individual *D. melanogaster* larvae. By collecting navigational statistics across populations of *D. melanogaster* larvae, we uncovered behavioral strategies.

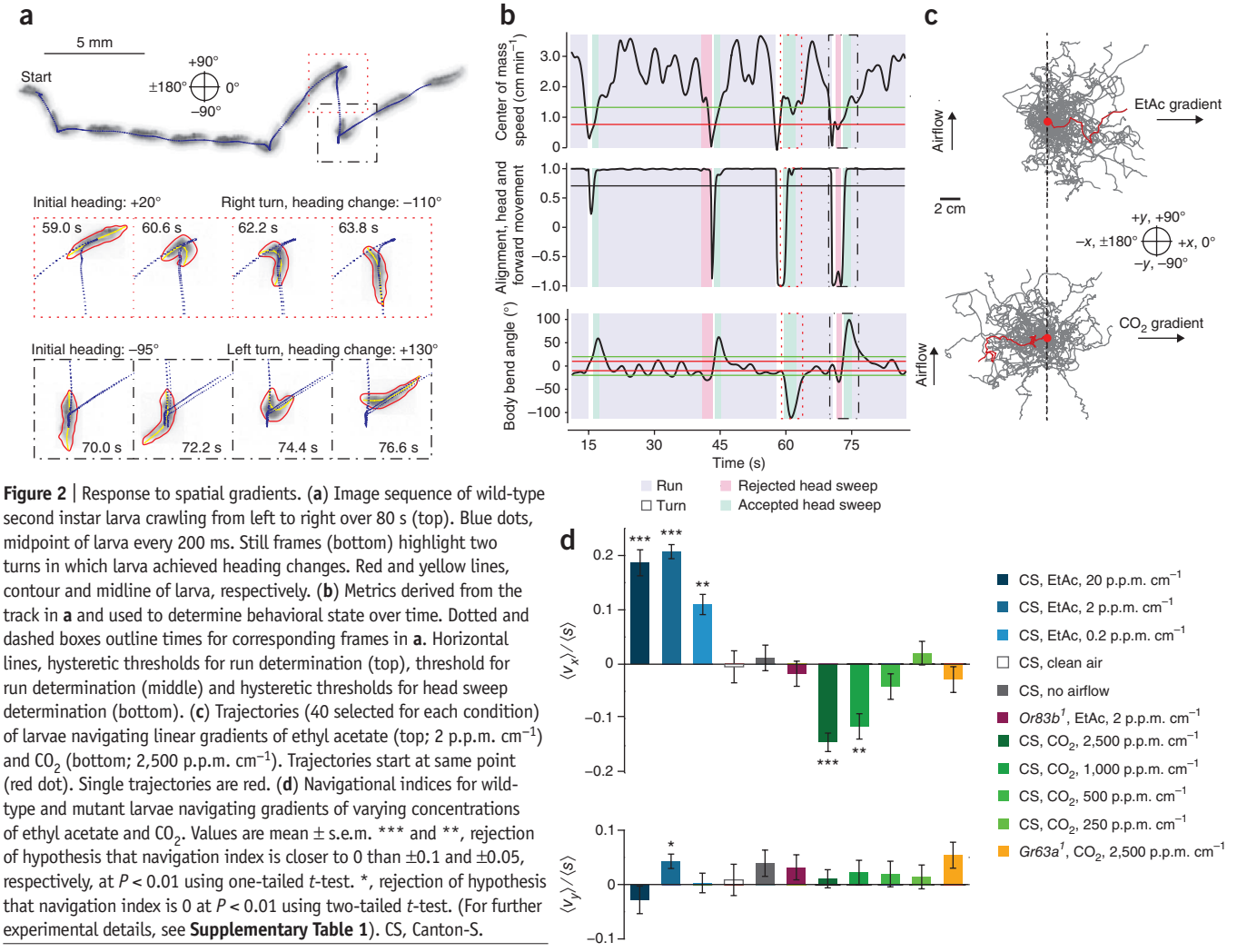

Figure 2 | Response to spatial gradients. (**a**) Image sequence of wild-type second instar larva crawling from left to right over 80 s (top). Blue dots, midpoint of larva every 200 ms. Still frames (bottom) highlight two turns in which larva achieved heading changes. Red and yellow lines, contour and midline of larva, respectively. (**b**) Metrics derived from the track in **a** and used to determine behavioral state over time. Dotted and dashed boxes outline times for corresponding frames in **a**. Horizontal lines, hysteretic thresholds for run determination (top), threshold for run determination (middle) and hysteretic thresholds for head sweep determination (bottom). (**c**) Trajectories (40 selected for each condition) of larvae navigating linear gradients of ethyl acetate (top; 2 p.p.m. cm^{-1}) and CO_2 (bottom; 2,500 p.p.m. cm^{-1}). Trajectories start at same point (red dot). Single trajectories are red. (**d**) Navigational indices for wild-type and mutant larvae navigating gradients of varying concentrations of ethyl acetate and CO_2. Values are mean ± s.e.m. *** and **, rejection of hypothesis that navigation index is closer to 0 than ±0.1 and ±0.05, respectively, at $P < 0.01$ using one-tailed *t*-test. *, rejection of hypothesis that navigation index is 0 at $P < 0.01$ using two-tailed *t*-test. (For further experimental details, see **Supplementary Table 1**). CS, Canton-S.

We characterized the navigational strategies of *D. melanogaster* larvae in response to ethyl acetate and CO_2 using defined spatial and temporal gradients. First, we examined the response to ethyl acetate, a volatile attractant[16], in linear spatial gradients with defined steepness[6]. We placed second instar Canton-S larvae in the middle of each gradient and quantified the resulting trajectories (**Fig. 2c**). Throughout this study, we used a compass in which 0° indicates movement up the gradient (+*x* direction), 180° indicates movement down the gradient (–*x* direction), +90° indicates movement downwind, orthogonal to the gradient (+*y* direction) and –90° indicates movement upwind, orthogonal to the gradient (–*y* direction). To quantify the overall navigational response in each linear spatial gradient, we computed a navigational index by dividing the mean velocity of all larvae in the *x* direction, $\langle v_x \rangle$, by the mean crawling speed, $\langle s \rangle$

$$Index = \langle v_x \rangle / \langle s \rangle \quad (1)$$

Hence, the navigational index was ±1 if the larvae crawled uniformly straight up or down the gradient and 0 if the movement was unbiased. This index (**Fig. 2d**) was significantly greater than zero ($P < 0.01$) across three ethyl acetate gradient steepnesses that we studied, indicating that chemotaxis toward ethyl acetate persists over two orders of magnitude in ethyl acetate concentration.

We did two control experiments without odorant, one in which the valves injected clean air into the laminar flow and one in which no laminar flow was provided (**Fig. 2d**). In both cases, the navigational index in the *x* direction was 0. We also tested *Orco*[1] larvae, which lack function in all olfactory neurons[16,17] and did not navigate ethyl acetate gradients (**Fig. 2d**).

Next, we examined the response to CO_2, a gaseous repellant[18], in linear spatial gradients with different steepnesses. The navigational indices were negative (indicating repulsion) and depended strongly on steepness (**Fig. 2d**). Reducing the steepness by 90% essentially abolished navigation away from CO_2. We verified that a loss-of-function mutation in Gr63a, a required CO_2 chemosensory receptor[13,18,19], disrupts CO_2 avoidance (**Fig. 2d**).

To assess whether the larvae responded to the laminar airflow itself (that is, exhibited rheotaxis), we computed the orthogonal navigational index, the mean velocity of all larvae in the *y* direction divided by the mean crawling speed (**Fig. 2d**). In all cases, orthogonal indices were ~0 and were not correlated with navigational indices in the gradient direction, indicating that airflow does not disrupt navigational response to the airborne cue.

Navigation in spatial gradients

What biases in the sequence of runs and turns along each trajectory enable the larvae to ascend ethyl acetate gradients (**Fig. 3**)

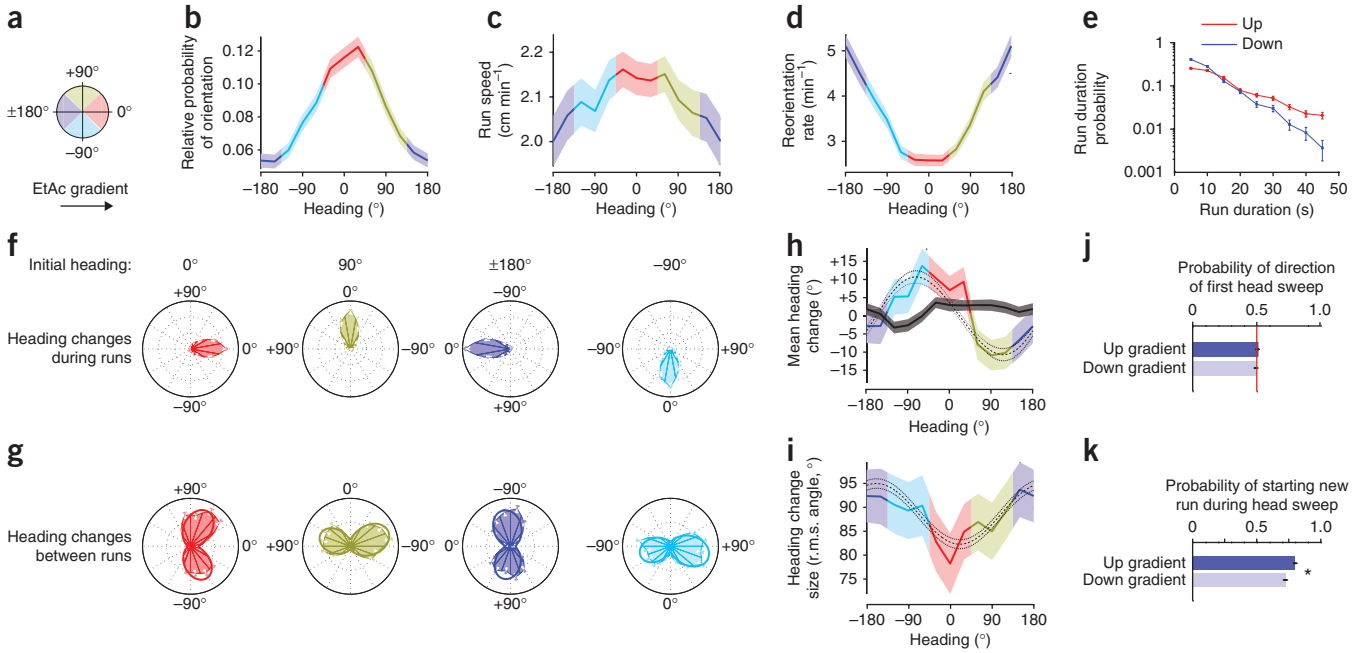

Figure 3 | Navigation of a 2 p.p.m. cm^{-1} ethyl acetate concentration gradient. (**a**) Schematic of heading angles; 0° is toward higher concentration. For data in this figure, ten experiments, 202 *D. melanogaster* larva and 29 h of behavior were analyzed. (**b**) Relative probability of headings during runs. (**c**) Speed versus heading during runs. (**d**) Turn rate versus heading. (**e**) Durations of runs headed up (1,537 runs) or down (1,091 runs) gradients. (**f**) Heading changes during runs sorted by initial heading: up gradients (red, 1,499 runs), orthogonal with higher concentration to right (gold, 1,354 runs), down gradients (blue, 1,062 runs) and orthogonal with higher concentration to left (cyan, 1,184 runs). (**g**) Heading changes achieved by turns, sorted as in **f** on the basis of heading immediately before the turn (0°, 1,201 reorientations; 90°, 1,214 reorientations; 180°, 1,105 reorientations; –90°, 1,049 reorientations). (**h**) Mean heading change achieved by runs (black line) versus initial heading and turns (colored line) versus heading before turn. Shaded regions indicate ± s.e.m. (**i**) r.m.s. turn angle versus run heading before turn. Dashed and dotted lines in **h**,**i** represent prediction and 95% confidence interval of model (Online Methods). (**j**,**k**) Statistics of head sweeps during turns after runs headed orthogonal to concentration gradient. Probability of direction of first head sweep (**j**; 1,967 head sweeps) and probability that larva initiates a new run during head sweeps (**k**; 2,341 head sweeps). Asterisk, rejection of hypothesis that probabilities are the same at $P < 0.01$ (Welch's *t*-test). Mean ± s.e.m. calculated as described in Online Methods (**b**,**c**), mean ± s.e.m. derived from counting statistics (**d**–**g**,**j**,**k**) and mean ± s.e.m (**h**,**i**).

and descend CO_2 gradients (**Fig. 4**)? We describe the motion of larvae during runs by the magnitude (run speed) and direction (run heading) of the velocity vector. We calculated the fraction of time that larvae spent crawling in different directions on linear spatial gradients by making a histogram of run heading, and found that larvae spent the most time moving up ethyl acetate gradients and down CO_2 gradients (**Figs. 3b** and **4b**). Larvae also crawled slightly faster when heading up ethyl acetate gradients than down and crawled slightly slower when heading up CO_2 gradients than down (**Figs. 3c** and **4c**).

We examined the rate at which larvae initiated turns as a function of heading on linear spatial gradients, and found that the probability of larvae initiating a turn per unit time on linear gradients of ethyl acetate or CO_2 (**Figs. 3d** and **4d**) was a smoothly varying function of heading with maximum at 180° or 0°, respectively. Thus, larvae extended runs in favorable directions, up gradients of ethyl acetate and down gradients of CO_2 (**Figs. 3e** and **4e**). This strategy, termed the biased random walk, is also exhibited during *Escherichia coli* chemotaxis[20].

D. melanogaster larvae have been proposed to directly orient toward higher attractant concentrations during periods of forward movement[8]. To investigate whether larvae steer within runs, we compared headings at the end and beginning of each run. If larvae were steering toward more favorable directions during runs, we would expect that, on average, runs would end with more favorable headings than they began. We examined the angle change during runs (final heading minus initial heading) as a function of initial headings (**Figs. 3f** and **4f**). The mean heading change (**Figs. 3h** and **4h**) during runs was nearly zero regardless of initial heading, so larvae did not seem to orient themselves during runs.

To examine whether larvae modulate the size and direction of turns to augment the number of runs in a favorable direction, we examined the heading change effected by each turn (**Supplementary Video 5**). When larvae turned after a run up or down either ethyl acetate or CO_2 gradients (**Figs. 3g** and **4g**), the heading change distributions were bimodal and roughly symmetric but narrower when larvae were initially headed in the favorable direction. When larvae turned after a run oriented perpendicular to the gradient, they did so with the same distribution of angular sizes to the left or right, but made more turns toward the favorable direction. For any given initial heading, the angular distribution of heading changes after turns could be modeled as the sum of two skew-normal distributions (Online Methods).

To quantify how turns enhance orientation during navigation, we measured the moments of heading-change distributions as functions of initial heading. In contrast to the mean zero heading change achieved during runs, the mean heading change after turns (**Figs. 3h** and **4h**) showed significant biases ($P < 0.01$ using the model described in Online Methods) to orient the larvae toward higher concentration of ethyl acetate or lower concentration of

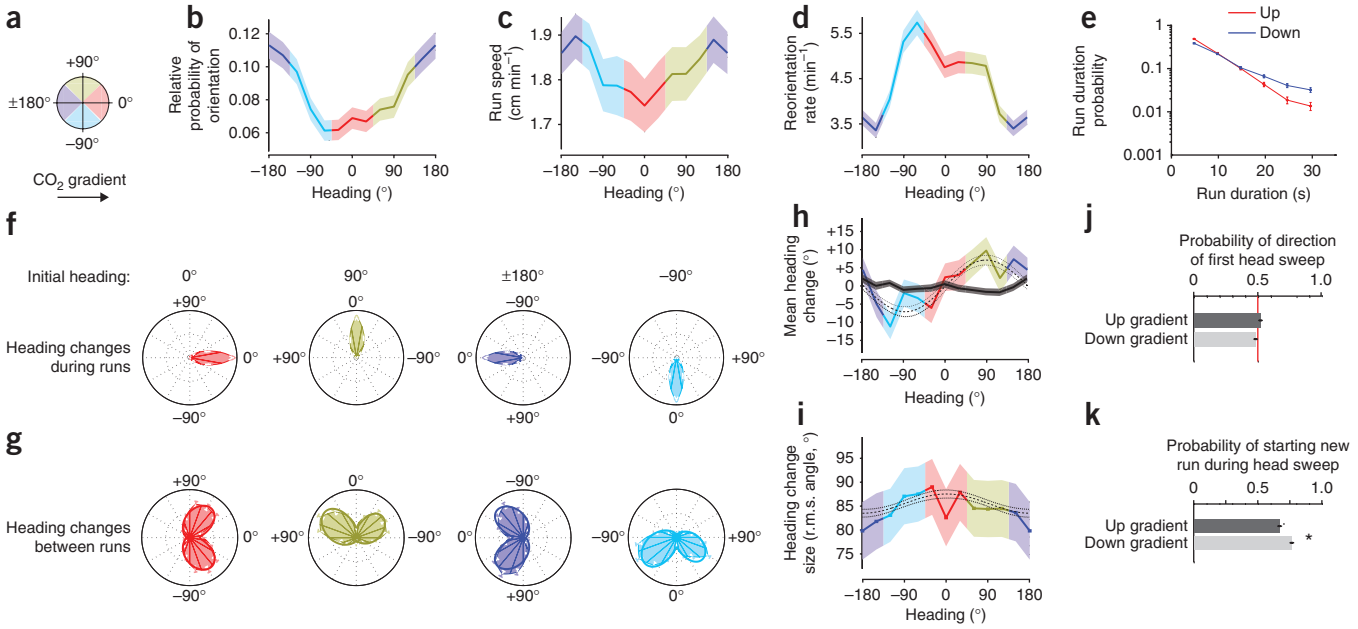

Figure 4 | Navigation of a 2,500 p.p.m. cm^{-1} CO_2 concentration gradient. (**a**) Schematic of heading angles; 0° is toward higher concentration. For data in this figure, 21 experiments, 168 *D. melanogaster* larva and 31 h of behavior were analyzed. (**b**) Relative probability of headings during runs. (**c**) Speed versus heading during runs. (**d**) Turn rate versus heading. (**e**) Durations of runs headed up (1,494 runs) or down (1,866 runs) gradients. (**f**) Heading changes during runs sorted by initial heading: up (red, 1,484 runs), down gradients (blue, 1,844 runs), orthogonal with higher concentration to right (gold, 1,651 runs) and orthogonal with higher concentration to left (cyan, 1,664 runs). (**g**) Heading changes achieved by turns, sorted as in **f** on the basis of heading immediately before the turn (0°, 1,196 reorientations; 180°, 1,336 reorientations; 90°, 1,306 reorientations; –90°, 1,375 reorientations). (**h**) Mean heading change achieved by runs (black line) versus initial heading and turns (colored line) versus heading before turn. (**i**) r.m.s. turn angle versus run heading before turn. Dashed and dotted lines in **h**,**i**, prediction and 95% confidence interval, respectively, of model described in Online Methods. (**j**,**k**) Statistics of head sweeps during turns after runs headed orthogonal to concentration gradient. Probability of direction of first head sweep (**j**; 2,497 head sweeps) and probability that the larva initiates a new run during head sweeps (**k**; 3,254 head sweeps). Asterisk, rejection of hypothesis that probabilities are the same at $P < 0.01$ (Welch's *t*-test). Mean ± s.e.m. calculated as described in Online Methods (**b**,**c**), mean ± s.e.m. derived from counting statistics (**d**–**g**,**j**,**k**) and mean ± s.e.m. (**h**,**i**).

CO_2 after orthogonal runs. The r.m.s. heading change (**Figs. 3i** and **4i**) showed larger heading changes in turns after runs pointed toward lower ethyl acetate concentration or toward higher CO_2 concentration.

During a turn, a larva sweeps its head to one side, after which it either starts a new run or initiates a new head sweep (**Fig. 2** and **Supplementary Video 6**). To uncover bias in these detailed head sweeping movements, we analyzed the statistics of all head sweeps initiated by larvae after runs pointed orthogonal to ethyl acetate or CO_2 gradients. In contrast to a recent report[9], we found that the direction of the initial head sweep in each turn was unbiased by gradient direction (**Figs. 3j** and **4j**). However, the larva more often initiated new runs during head sweeps that pointed in the favorable direction (**Figs. 3k** and **4k**).

Navigation in temporal gradients

The larva detects odors via the dorsal organ and CO_2 via the terminal organ[21]. Because right and left dorsal and terminal organs are separated by only ~10 µm, the larva probably detects spatial gradients by making temporal comparisons during its movements rather than by directly comparing the activity of the two sensory organs. Indeed, larvae with unilateral olfactory function exhibited chemotaxis toward volatile attractants[8] nearly as well as larvae with bilateral olfactory function.

We used our system to determine whether patterns of behavior exhibited on spatial gas gradients could be driven with temporal gradients of ethyl acetate or CO_2 concentration that were spatially uniform along the *x* axis (**Supplementary Fig. 2** and **Fig. 1d**). Triangular waveforms with linearly increasing and decreasing gas concentrations over time mimic the temporal stimulus experienced by a larva crawling in a straight line up or down a linear spatial gradient. When subjected to increasing concentration of CO_2 over time, larvae reoriented more frequently, crawled more slowly and turned with larger angles (**Fig. 5a**) than when the concentration was decreasing, consistent with our observations of larvae on spatial gradients (**Fig. 4c**,**d**).

We also explored sensorimotor response to CO_2 using step stimuli (**Fig. 5b**,**c**). We found that a small temporal step change (increase or decrease) in CO_2 concentration produced a transient increase or decrease, respectively, in turning rate. Large steps in CO_2 concentration were less adaptive, producing a sustained change in the turning rate. Very small concentration change (to 0.25%) did not affect turning rate but modulated crawling speed. Crawling speed was slow to adapt for small concentration changes and did not adapt at all for large concentration changes. The fact that turning rate adapted differently than crawling speed might indicate differences in the sensorimotor pathways between CO_2 detection and the circuits that regulate crawling speed and turn initiation.

To verify lack of adaptation to changes in CO_2, we extended the step waveform period to 480 s and still saw no evidence for adaptation in response parameters (**Fig. 5c**). Mutants lacking the *Gr63a* sensor for CO_2 modulated their behavior minimally in

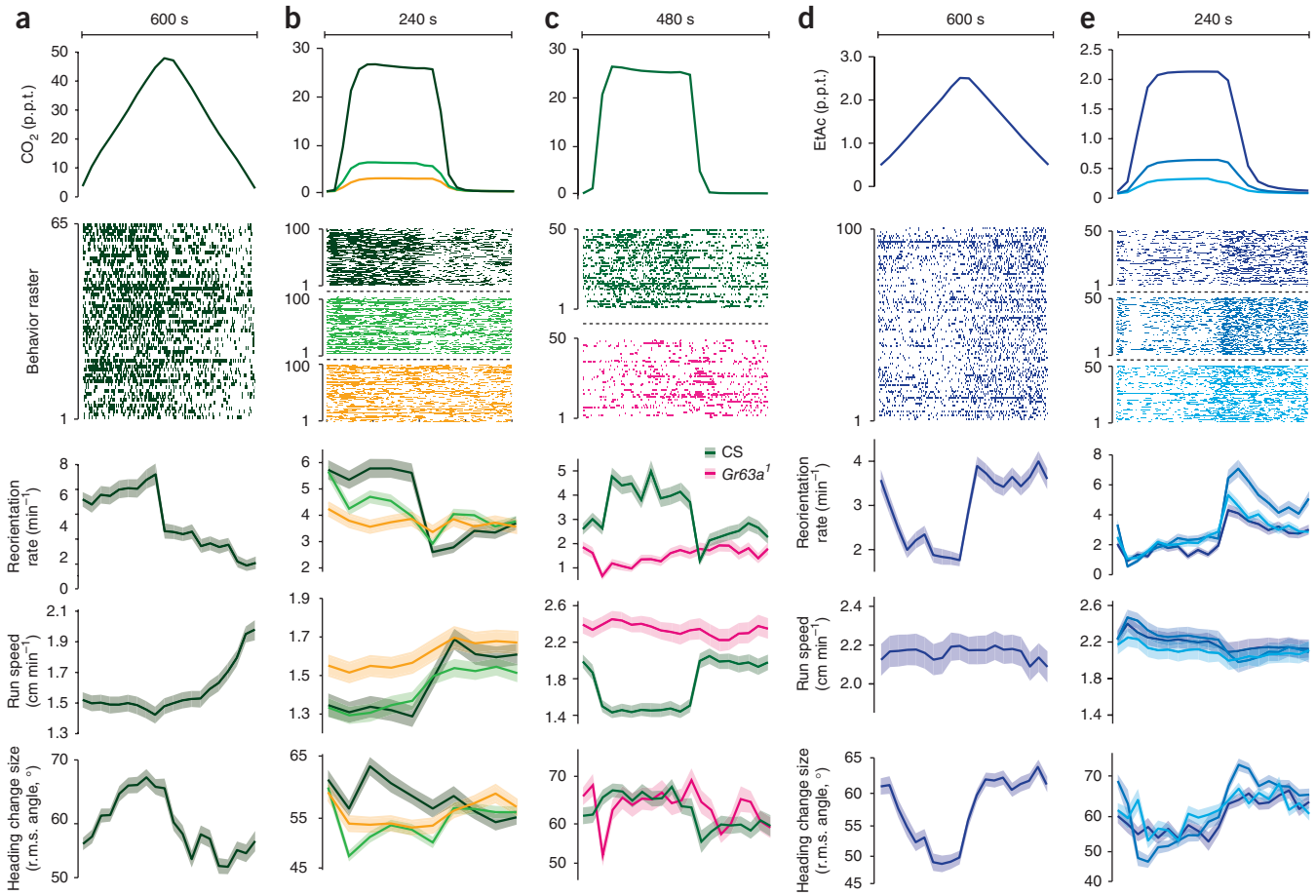

Figure 5 | Temporal CO_2 and ethyl acetate gradients. (**a**–**e**) Statistics of turning decisions of larvae subjected to spatially uniform temporal gradients of CO_2 delivered as repeating cycles of triangle waves (**a**) and steps (**b**,**c**) and of ethyl acetate delivered as triangle waves (**d**) and steps (**e**). Top, one cycle of stimulus waveform. Raster plots, periods in which an individual larva was turning during the cycle; each row represents one larva tracked continuously through a cycle (**a**, $n = 65$; **b**, $n = 100$ for each condition; **c**, $n = 50$ for each condition; **d**,**e**, $n = 100$ for each condition). Bottom, turning rate (mean ± s.e.m.) derived from counting statistics, mean crawling speeds ± s.e.m. calculated as described in Online Methods and root mean square heading change after turns ± s.e.m. versus time within each cycle. Data from wild-type larvae (CS) are in **a**,**b**,**d**,**e**. Step response of wild-type larvae and *Gr63a*^{1} mutant larvae are compared in **c**.

response to temporal changes in CO_2 concentration (**Fig. 5c**). Thus, CO_2-evoked changes in turning behavior and crawling speed were due to active sensorimotor responses and not a metabolic consequence of higher CO_2 concentration.

We examined larva behavior in temporal gradients of ethyl acetate. When larvae were subjected to a continuously increasing concentration of ethyl acetate over time, they reoriented less frequently and turned with smaller angles (**Fig. 5d**), consistent with their behavior on spatial gradients (**Fig. 3c**,**d**). Changes in crawling speed induced by linear ramps of ethyl acetate were not apparent (**Fig. 5d**). In contrast to the response to step changes in CO_2 (**Fig. 5b**,**c**), the response to step changes in ethyl acetate was adaptive across a wide range of concentrations (**Fig. 5e**). A temporal step increase or decrease in ethyl acetate concentration produced, respectively, a transient decrease or increase in the rate of turn initiation, slightly higher or lower crawling speeds and a transient decrease or increase in the size of turns (**Fig. 5e**).

DISCUSSION

Animals may sense the direction of a local gradient either directly, for example, by instantaneously comparing the activity of bilateral sensory organs or by decoding temporal signals generated by moving their sensory organs through the gradient. Here we found evidence for the latter for both odor and CO_2 gradients; larvae initiated turns more often when their forward movement caused an unfavorable change in concentration, and larvae based their turning decisions on the favorability of changes encountered during head sweeps, similar to our results in thermotaxis[13]. As in our studies of thermotaxis, we used time-varying spatially uniform signals to evoke behaviors observed in spatial gradients. We did not see signs of direct gradient measurement; specifically, larvae did not steer during runs and did not favor the preferred direction in the first head sweep of a turn.

In experiments involving odor and agar substrates, some odorant can be absorbed into the gel. Substantial odorant absorption into the substrate could affect stimulus presentation during temporal gradients, but as *D. melanogaster* larva responded consistently to abrupt changes in odor concentration over the course of our experiments, any effect of odorant absorption was modest. Our ability to present rapid changes in odor concentration was slightly compromised by the design of the reservoirs in the apparatus, but the 10–90% rise time for a step change (20.8 s) was smaller

than the bin sizes in **Figure 5** (**Supplementary Note 3**). The rise time can be decreased by redesigning the reservoirs or increasing the flow rate. In experiments in which we suddenly reversed the direction of the gradient (data not shown), larvae followed the new gradient direction rather than the old, also indicating that odorant absorption does not confound airborne navigation.

In navigation experiments, asymmetry with respect to the arena boundary can confound the results. For example, without stimulus, larvae placed at the left edge of a plate will show a navigational bias to the right because they are physically constrained from moving left. For this reason, we began each experiment with the larvae placed roughly in the center of the arena. Otherwise, as the spatial odor gradient in our apparatus is linear in the *x* direction, constant in the *y* direction and steady in time, experiments in our apparatus are less sensitive to initial placement of the larvae than droplet-based assays.

Our apparatus flexibly and accurately provided airborne stimulants to freely moving larva. Using this apparatus and machine-vision analysis that is sensitive to time-varying position and posture of each larva, we analyzed the algorithmic structure of navigational behavior with precision. We determined the navigational strategies of larvae in response to ethyl acetate and CO_2, showed internal consistency between their behavioral response to spatial gradients and temporal gradients, and uncovered a nonadaptive response for temporal changes in CO_2. The marked similarities between the algorithmic structure of navigational strategies during chemotaxis and thermotaxis suggest that homologous sensorimotor circuits might be used to encode larval navigation in response to diverse sensory inputs[15].

METHODS

Methods and any associated references are available in the online version of the paper at http://www.nature.com/naturemethods/.

Note: Supplementary information is available on the Nature Methods website.

ACKNOWLEDGMENTS

We thank E. Soucy and J. Greenwood for engineering advice and suggestions. This work was supported by a US National Institutes of Health (NIH) Pioneer award to A.D.T.S., NIH grants to J.R.C. and an NIH National Research Service award to E.A.K.

AUTHOR CONTRIBUTIONS

M.G. designed and constructed the linear and dynamic gaseous gradient apparatus, designed and wrote MAGAT analyzer software, designed and carried out experiments, analyzed all data and assembled figures. M.B. designed and carried out experiments. D.M. and L.L. designed and carried out preliminary experiments. E.A.K. designed experiments. J.R.C. and A.D.T.S. supervised the project and designed experiments. M.G., E.A.K. and A.D.T.S. wrote the manuscript.

COMPETING FINANCIAL INTERESTS

The authors declare no competing financial interests.

Published online at http://www.nature.com/naturemethods/.
Reprints and permissions information is available online at http://www.nature.com/reprints/index.html.

1. Brody, C.D. & Hopfield, J.J. Simple networks for spike-timing-based computation, with application to olfactory processing. *Neuron* **37**, 843–852 (2003).
2. Cleland, T.A. & Linster, C. Computation in the olfactory system. *Chem. Senses* **30**, 801–813 (2005).
3. Hopfield, J.J. Olfactory computation and object perception. *Proc. Natl. Acad. Sci. USA* **88**, 6462–6466 (1991).
4. Chalasani, S.H. *et al.* Dissecting a circuit for olfactory behaviour in *Caenorhabditis elegans*. *Nature* **450**, 63–70 (2007).
5. Masse, N.Y., Turner, G.C. & Jefferis, G.S. Olfactory information processing in *Drosophila*. *Curr. Biol.* **19**, R700–R713 (2009).
6. Bargmann, C.I., Hartwieg, E. & Horvitz, H.R. Odorant-selective genes and neurons mediate olfaction in *C. elegans*. *Cell* **74**, 515–527 (1993).
7. Kreher, S.A., Mathew, D., Kim, J. & Carlson, J.R. Translation of sensory input into behavioral output via an olfactory system. *Neuron* **59**, 110–124 (2008).
8. Louis, M., Huber, T., Benton, R., Sakmar, T.P. & Vosshall, L.B. Bilateral olfactory sensory input enhances chemotaxis behavior. *Nat. Neurosci.* **11**, 187–199 (2008).
9. Gomez-Marin, A., Stephens, G.J. & Louis, M. Active sampling and decision making in *Drosophila* chemotaxis. *Nat. Commun.* **2**, 441 (2011).
10. Chronis, N., Zimmer, M. & Bargmann, C.I. Microfluidics for *in vivo* imaging of neuronal and behavioral activity in *Caenorhabditis elegans*. *Nat. Methods* **4**, 727–731 (2007).
11. Lockery, S.R. *et al.* Artificial dirt: microfluidic substrates for nematode neurobiology and behavior. *J. Neurophysiol.* **99**, 3136–3143 (2008).
12. Albrecht, D.R. & Bargmann, C.I. High-content behavioral analysis of *Caenorhabditis elegans* in precise spatiotemporal chemical environments. *Nat. Methods* **8**, 599–605 (2011).
13. Jones, W.D., Cayirlioglu, P., Kadow, I.G. & Vosshall, L.B. Two chemosensory receptors together mediate carbon dioxide detection in *Drosophila*. *Nature* **445**, 86–90 (2007).
14. Cayirlioglu, P. *et al.* Hybrid neurons in a microRNA mutant are putative evolutionary intermediates in insect CO_2 sensory systems. *Science* **319**, 1256–1260 (2008).
15. Luo, L. *et al.* Navigational decision making in *Drosophila* thermotaxis. *J. Neurosci.* **30**, 4261–4272 (2010).
16. Larsson, M.C. *et al.* Or83b encodes a broadly expressed odorant receptor essential for *Drosophila* olfaction. *Neuron* **43**, 703–714 (2004).
17. Vosshall, L.B. & Hansson, B.S. A unified nomenclature system for the insect olfactory coreceptor. *Chem. Senses* **36**, 497–498. (2011).
18. Faucher, C., Forstreuter, M., Hilker, M. & de Bruyne, M. Behavioral responses of *Drosophila* to biogenic levels of carbon dioxide depend on life-stage, sex and olfactory context. *J. Exp. Biol.* **209**, 2739–2748 (2006).
19. Kwon, J.Y., Dahanukar, A., Weiss, L.A. & Carlson, J.R. The molecular basis of CO_2 reception in *Drosophila*. *Proc. Natl. Acad. Sci. USA* **104**, 3574–3578 (2007).
20. Berg, H.C. & Brown, D.A. Chemotaxis in *Escherichia coli* analysed by three-dimensional tracking. *Nature* **239**, 500–504 (1972).
21. Vosshall, L.B. & Stocker, R.F. Molecular architecture of smell and taste in *Drosophila*. *Annu. Rev. Neurosci.* **30**, 505–533 (2007).

ONLINE METHODS

Strains. Wild-type larvae were Canton-S (CS). *Gr63a*[1] (Bloomington stock 9941) and *Orco*[1] (Bloomington stock 23129) flies were obtained from the Bloomington stock center. *Orco* represents the new gene name for *Or83b*[17]. All behavioral experiments were done on second instar larvae. Adult flies were allowed to lay eggs on grape-juice agar growth plates with yeast for 3 h. After egg laying, plates were kept at 22 °C on a 12 h day-night cycle. Experiments were carried out at 22 °C during the day cycle or early hours of the night cycle. Time since egg laying was used to roughly stage larvae, and actual stage was verified by examining spiracle morphology.

Odor gradient apparatus. The odor gradient apparatus (**Fig. 1a**) comprises a controlled clean air source, an odor source, an array of microcontroller-activated valves, a mixing flow block and a laminar flow chamber. Compressed air was regulated to 140 kPa and cleaned with a charcoal filter (Agilent HT200-4) before delivery to a computer-controllable mass-flow controller (MFC; Aalborg GFC 17). A second MFC was used to inject airborne chemical stimulants into the laminar airflow. For ethyl acetate experiments, the second MFC injected air into a bubbler made up of a 250-ml glass bottle with a stainless steel cap and frit, containing ethyl acetate (Mallinckrodt) either pure or diluted in deionized water. This generated an odorized air stream with the concentration of ethyl acetate in the air determined by the concentration of ethyl acetate in the bubbler. The water-ethyl acetate mixture does not obey Raoult's Law, so the ethyl acetate vapor pressure of the mixture was measured directly using a photoionization detector (PID; Baseline-Mocon Pidtech Plus). For CO_2 experiments, pure CO_2 was metered using an MFC calibrated for CO_2.

The carrier air was injected into the rear of the mixing flow block. For temporally varying, spatially uniform stimuli (**Fig. 1d** and **Supplementary Fig. 2**), the outlet of the odor source was connected to the inlet of the mixing block at the same location as the carrier air. The total amount of odor in the chamber was set by adjusting the flow rate of odor while holding the carrier flow rate constant (generally 2 l min^{-1}). The odor concentration was monitored during each experiment at the inlet using either a PID or a nondispersive infrared CO_2 sensor (http://www.co2meter.com/, GSS C20).

For spatially varying, temporally uniform stimuli (**Fig. 1b**,**c**), the outlet of the odor source was connected to the inlet of the valve manifold. Compact solenoid valves (Lee, LHDA1221111H) were used to meter odor through a section of teflon tubing into each flow tube in the mixing block. The valves were controlled by a custom circuit board based on SpokePOV (Adafruit Industries) and were programmed to open for linearly increasing amounts of time over a period of ~1.5 s (**Supplementary Software 2**). The valves were operated in a pattern that kept exactly half open at any time, presenting a constant impedance to the MFC (**Supplementary Fig. 3**). The minimum continuous time a valve was opened or closed was therefore ~50 ms, whereas the valve switching time was 3 ms. The mean concentration of the gradient was set by varying the ratio of odor flow to carrier air flow and was monitored at the outlet of the flow chamber by the appropriate gas sensor.

Diffusion smooths odor profiles generated by the valves. Between the outlet of the mixing block and the start of the experimental arena, diffusion smooths the profile with a length scale of 1.2 cm for ethyl acetate and 1.7 cm for CO_2. By the far edge of the experimental arena, the smoothing length scale is 1.8 cm and 2.5 cm for ethyl acetate and CO_2, respectively. Thus, spatial irregularities owing to the discrete injection points are relaxed by the time the laminar airflow enters the arena, but the gradient itself is not dissipated before the airflow exits the arena.

The laminar airflow containing spatial or temporal gradients of ethyl acetate or CO_2 passed through an experimental arena made from a solid piece of black anodized aluminum. A glass lid provided a viewing window for observing behavior. A hinged, pneumatic compressor was used to press the glass ring against an O-ring, creating a reliable seal. The integrity of all O-ring seals (at the inlet, outlet and glass lid) was continuously verified by monitoring the airflow rate at the outlet.

Video microscopy of larvae within the experimental arena was done using dark-field illumination with red LEDs (624 nm, outside the range of larval phototaxis) that were mounted at the perimeter of the experimental arena. Video was recorded at 5 frames s^{-1} using a 5-megapixel USB camera (Mightex BCE-B050-U) and an 18-mm focal-length C-mount lens (Edmund Optics NT54-857). Each pixel in the captured images corresponded to a 0.063 mm × 0.063 mm square of the experimental arena.

Behavior experiments. Before each experiment, larvae were staged, washed in phosphate-buffered saline and placed on 10-cm Petri dish containing clean 1% (wt/vol) Bacto agar medium for at least 5 min to allow the larvae to adapt to the medium used in the experiments and shed any residual odorous contaminants. After each behavioral experiment, all larvae were discarded.

The substrate for the behavioral experiments was a ~4-mm-thick Bacto agar gel (1% wt/vol) on top of square, flat, black, anodized aluminum plates (24 cm × 24 cm). Each plate with the gel on top could be placed in the experimental arena, providing a large uniform substrate for the larvae to navigate without edges to impede or distort airflow. Larvae were transferred from 10-cm Petri dishes to experimental arena using a paintbrush, the chamber was pneumatically sealed and the entire apparatus was enclosed in a light-tight box. After the chamber was pneumatically sealed, it took ~30 s for the laminar airflow to fully purge the chamber and establish a defined spatial gradient. We discarded the first 2 min of recorded behavior during analysis. We recorded behavior for 25–30 min per experiment; for experiments involving spatial gradients, we analyzed the first 15 min (after the discarded 2 min), after which larvae started nearing the edges of the gradients.

Behavioral analysis. The MAGAT analyzer software package is available as **Supplementary Software 1** or the latest version, with example video recordings, is available at https://github.com/samuellab/MAGATAnalyzer.

Larval positions and postures were extracted from video records using custom machine vision software written in C++ and based on OpenCV, an open-source computer vision software suite. With similar features to software that has been written to automatically follow *C. elegans* behavior[22–25], our software tracks each larva throughout the arena and records an image of the larva, the position of center of mass, the outline of the body, the position of the head and tail and a midline running down the center of the larva (**Fig. 2a** and **Supplementary Fig. 1** and **Supplementary Note 3**). Using data analysis software written in MATLAB (MathWorks),

doi:10.1038/nmeth.1853

we analyzed navigational statistics such as path curvature, speed, heading and angle of head relative to body (**Fig. 2b**). These were used to segment trajectories into an alternating sequence of runs and turns.

To calculate statistics involving center-of-mass movement along larval trajectories (for example, distributions of instantaneous heading and speed in **Figs. 3b**,**c** and **4b**,**c** and navigational indices in **Fig. 2d**) we needed to estimate the number of independent observations of quantities of center-of-mass movement along each larval trajectory. To do this, we calculated the autocorrelation function of the direction of motion,

$$C(\tau) = \left\langle \hat{v}(t) \cdot \hat{v}(t+\tau) \right\rangle_t \quad (2)$$

and extracted the time constant, T, of its component of exponential decay,

$$C(\tau) \approx e^{-\tau/T} \quad (3)$$

This correlation time constant was typically ~20 s. To calculate the s.e.m. of center-of-mass motion statistics, we estimated the number of independent observations as the total observation time for each measurement divided by twice the correlation time constant[23].

To calculate statistics of decision making along trajectories, trajectories were segmented into a sequence of alternating runs and turns. Runs (**Supplementary Video 4**) were defined as continuous periods of forward movement with head direction aligned with direction of forward travel (**Fig. 2b**). A hysteretic threshold for run speed was determined on an individual *D. melanogaster* larva basis by examining the speed near points of high curvature in the path; the speed to begin a run was higher than the speed to end one. The head was considered aligned with the direction of forward motion if the angle between the mid-head vector and the heading was <37°. Turns separated successive runs. The initiation of each head sweep (**Supplementary Video 6)** during a turn was flagged when the body bend angle between the anterior and posterior of the *D. melanogaster* larva was >20° (**Fig. 2b**). Each head sweep ended when the body bend angle was <10° or changed sign (head swept to other side of body) or when a new run began. Each turn ended at the start of a new run. Thus, each turn could involve zero or more head sweeps. Turns with zero head sweeps (pauses) were excluded from the statistics of reorientation after turns. Rare head sweeps in which the body bend angle was so extreme that the head touched the tail created difficulty during feature extraction because the tracker could no longer effectively distinguish head from tail. These head sweeps were also excluded from statistical analysis.

Video records of each larva along its trajectory could be played back, overlaid by extracted contour, head and tail locations, and path with annotations noting runs, turns and head sweeps (**Supplementary Videos 2** and **3**). A subset of these videos was examined visually to verify the performance of automated segmentation and analysis of larval trajectories.

Statistical model for heading change distributions after turns. To describe the distribution of heading changes after turns, we developed a statistical model to represent our observation that heading changes, $\Delta\theta$, are biased in size and direction by head sweeping movements and contingent on the initial heading on spatial gradients before each turn, θ_i. In this model, the magnitude of heading change is drawn from skew-normal distributions whose mean and skewness depend on θ_i, thereby allowing the size of turns to depend on initial heading on spatial gradients as observed. The direction of heading change (to the left ($\Delta\theta > 0$) or right ($\Delta\theta < 0$)) is determined by a biased coin-flip distribution whose mean depends on θ_i, thus biasing the likelihood of initiating new runs to the left or right

$$\begin{aligned} P(\Delta\theta|\theta_i) = &\left(\frac{1}{2} - A\sin(\theta_i - \theta_0)\right) \times SN\left(\Delta\theta, \mu - B\cos(\theta_i - \theta_0),\right. \\ &\left.\sigma, \alpha - C\cos(\theta_i - \theta_0)\right) + \left(\frac{1}{2} + A\sin(\theta_i - \theta_0)\right) \\ &\times SN\left(-\Delta\theta, \mu - B\cos(\theta_i - \theta_0), \sigma, \alpha - C\cos(\theta_i - \theta_0)\right) \end{aligned} \quad (4)$$

where

$$SN(x, \mu, \sigma, \alpha) = \frac{e^{-\frac{(x-\mu)^2}{2\sigma^2}}}{\sigma\sqrt{2\pi}} Erfc\left(\frac{-\alpha(x-\mu)}{\sigma\sqrt{2}}\right) \quad (5)$$

We adjusted the parameters of the model (A, B, C, μ, σ, α and θ_0) to maximize the likelihood of the observed initial heading-heading change pairs. The solid lines overlaying the histograms in **Figures 3h** and **4h** and dashed lines overlaying the plots of heading change magnitude and direction in **Figures 3e**,**f** and **4e**,**f** represent predictions of the model fit (equations (4) and (5)) to the experimental data.

For both ethyl acetate and CO_2, we assessed the statistical model represented by equations (4) and (5) by also calculating the maximum likelihood of observed data given null models that eliminated certain features from the full statistical model by setting one or more parameters to zero. We computed the logarithm of the ratios of maximum likelihood for the null model and full statistical model. These results are summarized in **Supplementary Table 2**. All null models could be rejected in favor of the full statistical model at $P < 0.01$.

22. Baek, J.H., Cosman, P., Feng, Z., Silver, J. & Schafer, W.R. Using machine vision to analyze and classify *Caenorhabditis elegans* behavioral phenotypes quantitatively. *J. Neurosci. Methods* **118**, 9–21 (2002).
23. Cronin, C.J., Feng, Z. & Schafer, W.R. Automated imaging of *C. elegans* behavior. *Methods Mol. Biol.* **351**, 241–251 (2006).
24. Swierczek, N.A., Giles, A.C., Rankin, C.H. & Kerr, R.A. High-throughput behavioral analysis in *C. elegans*. *Nat. Methods* **8**, 592–598 (2011).
25. Ramot, D., Johnson, B.E., Berry, T.L.J., Carnell, L. & Goodman, M.B. The Parallel Worm Tracker: a platform for measuring average speed and drug-induced paralysis in nematodes. *PLoS ONE* **3**, e2208 (2008).